



**HAL**  
open science

## Hydration of $Ti_3C_2T_x$ MXene: An Interstratification Process with Major Implications on Physical Properties

Stephane Celerier, S. Hurand, Cyril Garnero, Sophie Morisset, Mohamed Benchakar, Aurélien Habrioux, Patrick Chartier, Vincent Mauchamp, Nathaniel Findling, Bruno Lanson, et al.

### ► To cite this version:

Stephane Celerier, S. Hurand, Cyril Garnero, Sophie Morisset, Mohamed Benchakar, et al.. Hydration of  $Ti_3C_2T_x$  MXene: An Interstratification Process with Major Implications on Physical Properties. *Chemistry of Materials*, 2019, 31 (2), pp.454-461. 10.1021/acs.chemmater.8b03976 . hal-02183208

**HAL Id: hal-02183208**

**<https://hal.science/hal-02183208>**

Submitted on 15 Jul 2019

**HAL** is a multi-disciplinary open access archive for the deposit and dissemination of scientific research documents, whether they are published or not. The documents may come from teaching and research institutions in France or abroad, or from public or private research centers.

L'archive ouverte pluridisciplinaire **HAL**, est destinée au dépôt et à la diffusion de documents scientifiques de niveau recherche, publiés ou non, émanant des établissements d'enseignement et de recherche français ou étrangers, des laboratoires publics ou privés.

# Hydration of $\text{Ti}_3\text{C}_2\text{T}_x$ MXene: an interstratification process with major implications on physical properties

Stéphane Célérier,<sup>\*,†</sup> Simon Hurand,<sup>‡</sup> Cyril Garnero,<sup>†,‡</sup> Sophie Morisset,<sup>†</sup> Mohamed Benchakar,<sup>†</sup>  
Aurélien Habrioux,<sup>†</sup> Patrick Chartier,<sup>‡</sup> Vincent Mauchamp,<sup>‡</sup> Nathaniel Findling,<sup>§</sup> Bruno Lanson,<sup>§</sup>  
Eric Ferrage<sup>\*,†</sup>

<sup>†</sup> Institut de Chimie des Milieux et Matériaux de Poitiers (IC2MP), Université de Poitiers,  
CNRS, F-86073 Poitiers, France

<sup>‡</sup> Institut Pprime, UPR 3346 CNRS, Université de Poitiers, ISAE-ENSMA, BP 30179, 86962  
Futuroscope-Chasseneuil Cedex, France

<sup>§</sup> Univ. Grenoble Alpes, Univ. Savoie Mont Blanc, CNRS, IRD, IFSTTAR, ISTerre, F-38000  
Grenoble, France

## ABSTRACT

The MXenes, among which  $\text{Ti}_3\text{C}_2\text{T}_x$  is the most studied, are a large family of 2D materials with proven potential in a variety of application fields (*e.g.*, energy storage and conversion, water purification, electromagnetic interference shielding, humidity sensor, etc). For most of these applications, MXenes properties depend, at least partly, on their water sorption ability and on the induced structural swelling, which is commonly considered a stepwise process, like in clay-like materials. In the present study, we rather evidence the systematic coexistence of different hydrates in MXene interstratified crystals. Hydration heterogeneity and related structure disorder are described from the quantitative analysis of X-ray diffraction data. This specific methodological approach allows disentangling the complex interstratification and rationalizing the prediction of MXene electrical properties. The widespread use of this approach paves the way for a systematic and thorough determination of MXene structure, including order-disorder, and thus for grasping the influence of structural disorder (hydration heterogeneity) on a large number of MXene physical properties (*e. g.* optical transparency, capacitance). Deciphering this complex structural disorder is also essential in the design of new MXene-based materials for a variety of applications (supercapacitors, batteries, water treatment...).

## INTRODUCTION

Two-dimensional (2D) materials, defined as crystals with very high aspect ratios and a thickness limited to a few atomic layers, have attracted extensive attention due to their promising practical applications and fundamental values with enhanced or new properties as compared to their bulk counterparts.<sup>1</sup> Since the discovery of graphene,<sup>2</sup> other 2D materials, such as hexagonal boron

nitrides, transition metal dichalcogenides, metal oxides and hydroxides have thus been extensively investigated.<sup>1</sup> In this constellation of 2D materials, MXenes form a new attractive family.<sup>3,4</sup> These materials consist in  $M_{n+1}X_n$  octahedral layers ( $n = 1$  to  $3$ ) which are obtained by the exfoliation of the A element from  $M_{n+1}AX_n$  precursors, a family of 70+ known ternary carbides and nitrides, the so-called MAX phases (M = transition metal, A: group III-A or IV-A elements, X: C and/or N).<sup>5</sup> The exfoliation results in the surface passivation of the  $M_{n+1}X_n$  layers with different T terminal groups (OH, F, O ...) which significantly modify their properties.<sup>3-6</sup> The wide range of possible substitutions in the M, X (core), and T (surface) sites leads to a large family of 2D  $M_{n+1}X_nT_x$  materials with tunable properties opening an immense and largely unexplored field of potential applications. Although discovered recently,<sup>7</sup> the interest for MXenes and MXene-based composites is growing rapidly due to their outstanding properties with very promising perspectives in domains such as electromagnetic interference shielding,<sup>8</sup> supercapacitors,<sup>4</sup> batteries,<sup>9</sup> catalysis,<sup>10</sup> photocatalysis,<sup>11</sup> hydrogen storage,<sup>12</sup> biosensors,<sup>13</sup> transparent conductive films,<sup>14</sup> electromechanical actuators,<sup>15</sup> or separation and purification.<sup>16,17</sup> The properties and potential applications of these materials have been recently reviewed.<sup>3,9,18-20</sup>

Contrary to hydrophobic graphene,  $Ti_3C_2T_x$  MXenes have a macroscopic hydrophilic behavior close to that of clay materials depending on the etching agent used.<sup>4,21</sup> Indeed, water and cations, stabilized by the negative charge of the surface groups, can be intercalated between the MXene layers. The resulting layered structure induces on the experimental X-ray diffraction (XRD) patterns of oriented powders the presence of intense  $00l$  reflections, as for clay materials.<sup>22</sup> As highlighted by Ghidui et al.,<sup>21</sup> a discontinuous structural expansion in the direction normal to the basal planes is observed with increasing relative humidity (RH), as reported for clays.<sup>23,24</sup> Expansion, or swelling, is due to the intercalation of one and two planes of

water molecules at low RH and high RH conditions as described on Figure 1 ( $\text{Li}^+$  is displayed as inserted cation) and associated to monohydrated (1W) or bihydrated (2W) states of the crystal structure, respectively. This simplified description overlooks, however, the presence of hydration heterogeneities resulting from the coexistence of layers with different hydration states within the same crystals, especially in the transition domain between two “homogeneous” hydration states.

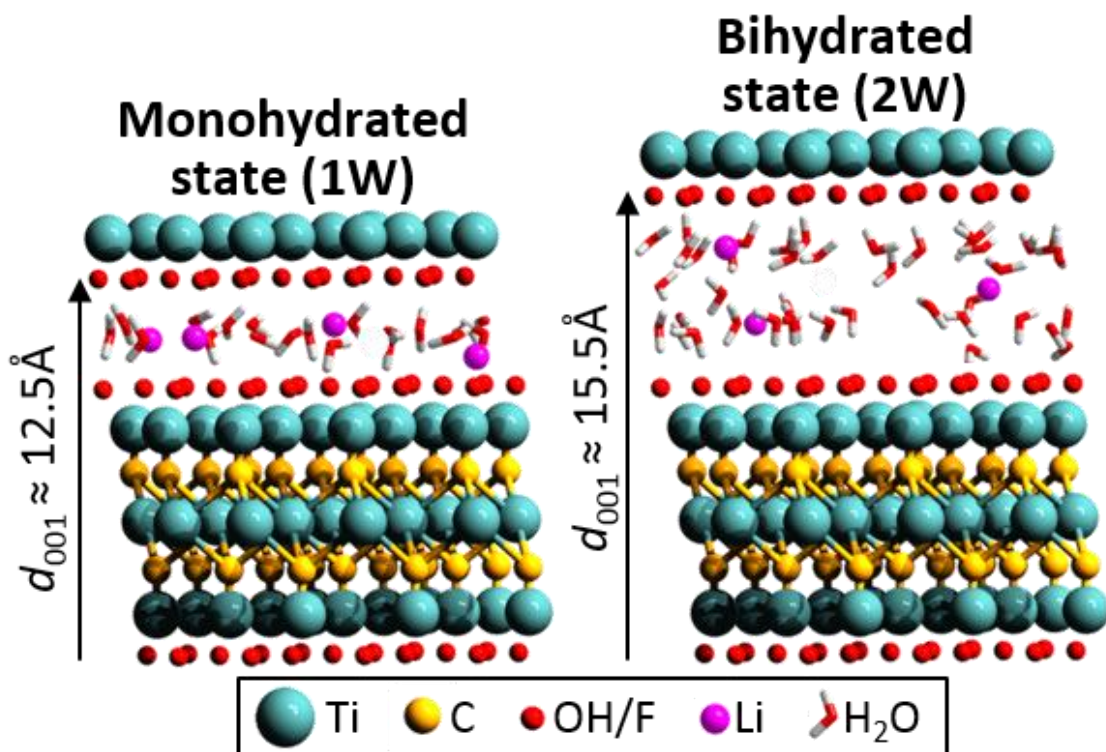


**Figure 1.** Structure models for monohydrated (1W) and bihydrated (2W)  $\text{Ti}_3\text{C}_2\text{T}_x$  MXene layers and respective typical  $d_{001}$  values (considering a one-layer unit cell).

Accounting for the crystalline disorder in MXene resulting from hydration heterogeneity is key however to numerous applications where MXene hydration can control the overall properties of the material, such as sorption efficiency,<sup>21</sup> insertion ability,<sup>25</sup> permeability,<sup>16</sup> conductivity,<sup>26</sup> capacitance,<sup>4,26,27</sup> ionic transport,<sup>20</sup> electrochemical,<sup>17,27</sup> elastic,<sup>20</sup> and optical properties.<sup>28</sup>

In the present study, a thorough description of the hydration of  $\text{Ti}_3\text{C}_2\text{T}_x$ , by far the most studied MXene to date, is proposed based on the detailed modeling of XRD data as a function of RH. The selected intercalated cation is  $\text{Li}^+$  since this ion is spontaneously intercalated between  $\text{Ti}_3\text{C}_2$  layers during the synthesis of the clay-like MXene developed by Ghidui et al.<sup>4</sup> and is well-adapted to study the ion-exchange and cation solvation in  $\text{Ti}_3\text{C}_2$ .<sup>21</sup> Influence of hydration heterogeneity on the resistivity response is then substantiated, in an effort to illustrate the need for a quantitative description of hydration to quantify its effect on MXene properties.

## RESULTS AND DISCUSSION

**Emphasis on structural rearrangement under various humidity.** XRD experiments under different RH conditions were performed on oriented MXene films prepared on glass slides from the initial  $\text{Ti}_3\text{C}_2\text{T}_x$  powder (XRD characterization of the powder is shown in Figure S1) to enhance 00 $l$  reflection intensity. Experimental XRD patterns reported in Figure 2 display a shift of the main diffraction peak from  $\sim 15.9$  to  $\sim 12.4$  Å when decreasing RH. Considering a unit cell composed by one  $\text{Ti}_3\text{C}_2$  layer and an interlayer space, these two peaks correspond to the 001 reflection of 2W and 1W MXene, respectively (Figure 1).<sup>21</sup> The transition between the two hydration states occurring over the 60-45% RH range (Figure 2), consistent with the results of Ghidui et al.,<sup>21</sup> is commonly associated to an abrupt transition of interlayer water filling. Some amounts of 1W layers are present even at high RH conditions, however, as shown by the shoulder at  $\sim 12$  Å visible even on the XRD pattern recorded at 95% RH (Figure 2). This diffraction feature is consistent with XRD data of Ghidui et al.<sup>21</sup> on Li-based MXene and pleads for a complex evolution of MXene hydration with RH and for the coexistence of 1W and 2W layers over an extended RH range.

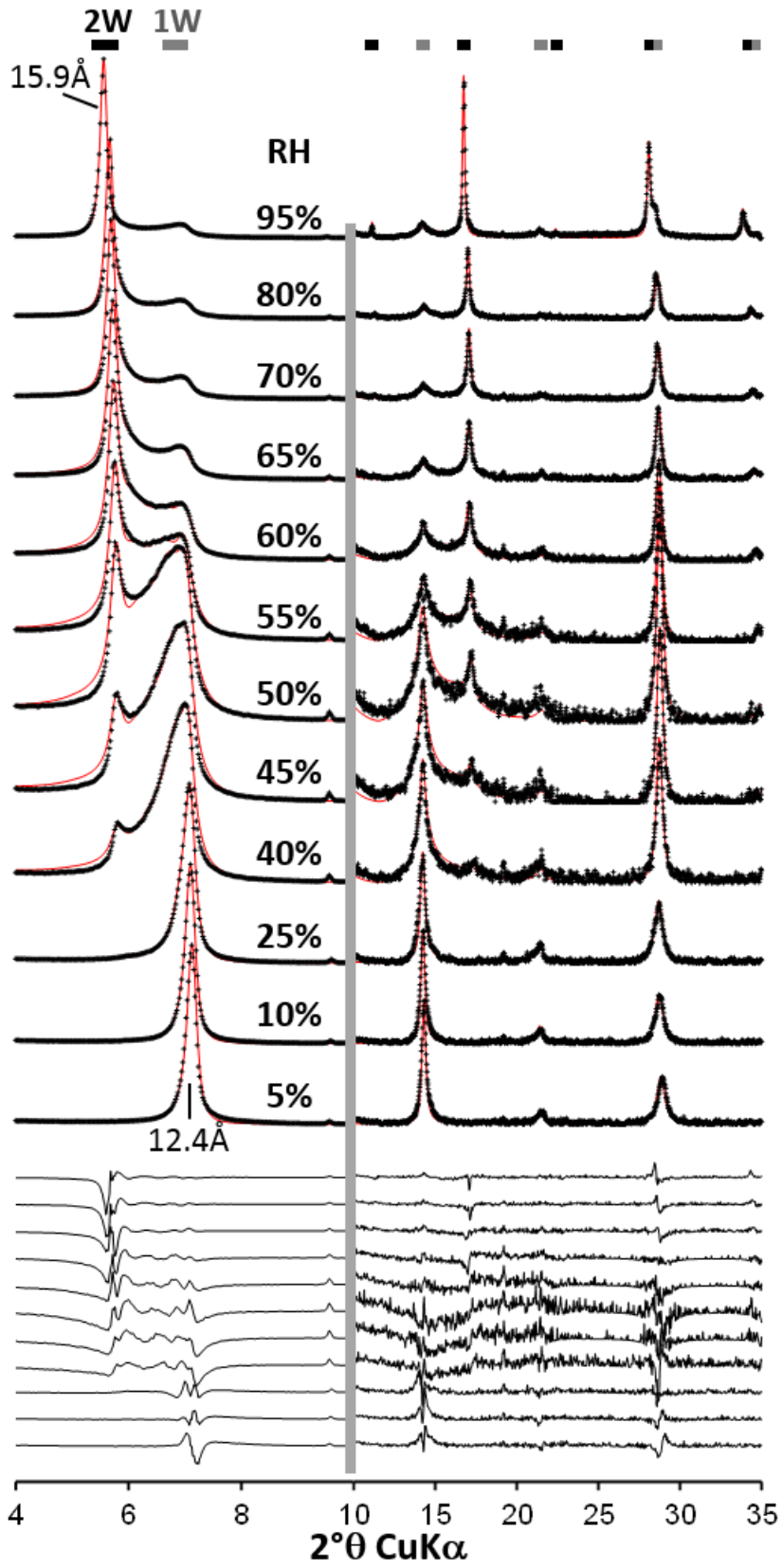


**Figure 2.** Comparison between experimental (black crosses) and calculated (red lines) intensities of  $00l$  reflections for Li-saturated  $\text{Ti}_3\text{C}_2\text{T}_x$  MXene as a function of relative humidity (RH). Difference plots are shown at the bottom of the figure. The vertical gray bar indicates a modified intensity scale factor ( $\times 30$ ) for the high-angle region of the patterns. At the top of the figure, solid black and gray boxes indicate typical positions for  $00l$  reflections of periodic 2W and 1W MXenes, respectively.

Hydration heterogeneity and related order/disorder in MXene samples can be probed through the analysis of peak positions and profiles of the entire series of  $00l$  reflections. For example, the  $00l$  reflections related to 1W and 2W contributions both shift in position indicating for a given hydration state a gradual decrease of the layer-to-layer distance, and hence of the water content, with decreasing RH (Figure 2). Over the 55-40 RH range, the 001 reflection associated to 1W layers is significantly broadened and shows a marked asymmetry on its low-angle side. An increased intensity of a diffuse asymmetric background is also visible over the  $13\text{-}18^\circ 2\theta$  angular range, in between the positions typical for periodic 2W and 1W MXenes. The variations in peak positions and widths for  $00l$  reflections between that typically expected for periodic 2W and 1W MXenes indicate the presence of interstratified structures, that is the coexistence of different hydration states within the same crystals, as commonly reported for hydrated swelling clay minerals.<sup>29</sup>

Quantitative description of such interstratified structures, or mixed layers, implies the use of specific XRD routines with an explicit description of crystals composed of layers having different layer-to-layer distances, compositions, and/or structures. Diffracted intensity for such mixed layers can be calculated based on the matrix formalism:<sup>30</sup>



$$I = N \text{Spur}[V][W] + 2 \text{Re} \sum_{n=1}^{N-1} (N-n) \text{Spur}[V][W][Q]^n \quad (1)$$

where  $N$  is the number of layers in a given crystal,  $[V]$  is a matrix containing the products of the structure factor amplitudes  $F_i^* F_j$  of the  $i^{\text{th}}$  and  $j^{\text{th}}$  layer types, depending on the amount and nature of elements present in the unit cells;  $[W]$  is the diagonal matrix with occurrence probabilities for single layers, layer pairs, triplets, and so on, depending on the order parameter defined by the Reichweite parameter  $R$ ; <sup>31</sup>  $[Q]$  is a square matrix with the products of the junction probabilities and of the associated phase term;  $\text{Re}$  is the real part of the complex; and  $\text{Spur}$  is the trace of the matrix, i.e., the sum of its diagonal elements. The order of the matrices  $[V]$ ,  $[W]$ , and  $[Q]$  depends on the number of layer types in the mixed layers and on the Reichweite parameter  $R$ , a parameter that describes how many of its neighbors will influence the presence of a given layer.

Calculation of diffraction effects for mixed layers with two layer types (here 1W and 2W layers) and for Reichweite parameter  $R = 1$  (the presence of a given layer is only influenced by the nature of its nearest neighbor) requires describing the stacking sequences of the different layer types. For this purpose it is necessary to determine the relative proportions of 1W and 2W layers (i.e.,  $W_{1W}$  and  $W_{2W}$ ) and junction probability parameters. These probability parameters, based on Markovian statistics and usually denoted  $P_{ij}$ , <sup>30</sup> account for the probability of finding a layer type ( $j$ ) after a given layer type ( $i$ ) ( $P_{1W-1W}$ ,  $P_{1W-2W}$ ,  $P_{2W-1W}$ , and  $P_{2W-2W}$  in the present case). Accordingly, 6 parameters ( $W_{1W}$ ,  $W_{2W}$ ,  $P_{1W-1W}$ ,  $P_{1W-2W}$ ,  $P_{2W-1W}$  and  $P_{2W-2W}$ ) are required to calculate the diffracted intensities for such two-component mixed layers. These parameters are connected by the following relations:

$$W_{1W} + W_{2W} = 1 \quad (2)$$

$$P_{1W-1W} + P_{1W-2W} = 1 \text{ and } P_{2W-1W} + P_{2W-2W} = 1 \quad (3)$$

$$W_{1W}P_{1W-2W} = W_{2W}P_{2W-1W} \quad (4)$$

Using these relations, plotting  $P_{1W-1W}$  as a function of  $W_{1W}$  allows describing the whole range of possible stacking sequences for a two-component mixed layer with  $R = 1$  (Figure 3).<sup>32</sup> Irrespective of  $W_{1W}$ , the line  $P_{1W-1W} = 1$  corresponds to the physical mixture of periodic 1W and 2W crystals, 1W and 2W layers being present in different crystals. On the other hand, when  $P_{2W-2W} = 0$  for  $W_{1W} > W_{2W}$  there is no possibility of finding pairs of the minor layer type (2W in this case) in the crystals. This corresponds to the so-called maximum possible degree of ordering (MPDO) for  $R = 1$ , which defines the relation  $P_{1W-1W} = (2 \times W_{1W} - 1) / W_{1W}$  ( $W_{1W} > W_{2W}$ ) according to relations 2-4. The specific point of this curve defined by  $W_{1W} = 0.5$  and  $P_{1W-1W} = 0$  corresponds to the regular and systematic alternation of 1W and 2W layers in all crystals. The last typical category of mixed layers is defined by the relation  $P_{1W-1W} = W_{1W}$  and corresponds to the random interstratification of 1W and 2W layers in the crystals. In this case, the probability to find a layer does not depend on the nature of the previous one ( $R = 0$ ), but only on its relative abundance. Figure 3 shows XRD patterns calculated for these three categories of mixed layers (i.e., physical mixture, random and MPDO interstratification) assuming identical proportions of 1W and 2W layers (1:1 ratio). For the physical mixture case (Figure 3A), the resulting XRD pattern corresponds to the sum of the  $00l$  reflection series of both 1W and 2W periodic structures. Note that despite their equal abundances, the relative intensities of the 001 reflection significantly differs for 1W and 2W layers due to the intensity distribution of their respective structure factors. In the case of random interstratification (Figure 3B), the calculated diffraction pattern displays peaks in positions intermediate between those expected for periodic 1W and 2W structures. In addition, peak breadth depends not only on the size of coherent scattering domains but increases also with the distance between neighboring  $00l$  reflections corresponding to

periodic 1W and 2W structures.<sup>33</sup> This results, for example, in a significant broadening of the diffraction bands at  $\sim 6.3$  and  $\sim 15.3^\circ 2\theta$  whereas the band at  $\sim 28.8^\circ 2\theta$  remains sharp. For MPDO interstratification (Figure 3C), the calculated XRD pattern exhibits a rational series of reflections corresponding to a 1W-2W super-cell. Those three examples illustrate the major influence of order/disorder on XRD patterns for a unique mixed-layer composition (i.e.,  $W_{1W} = 0.5$ ). Moreover, this presentation is limited to typical cases but intermediate cases such as partial segregation or partial ordering can also lead to significant variations of  $00l$  reflection profiles.

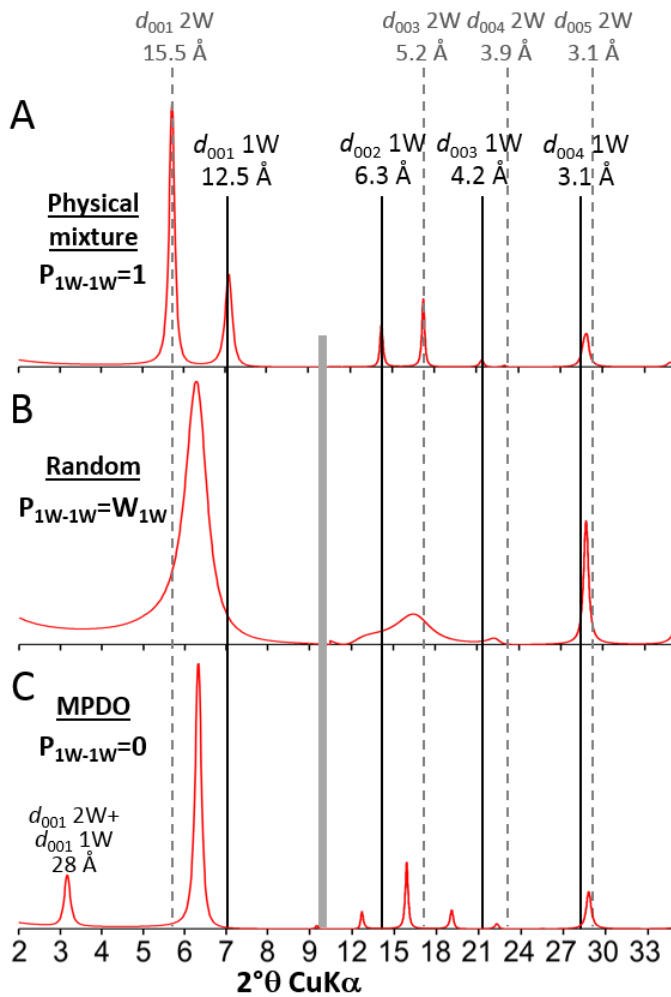
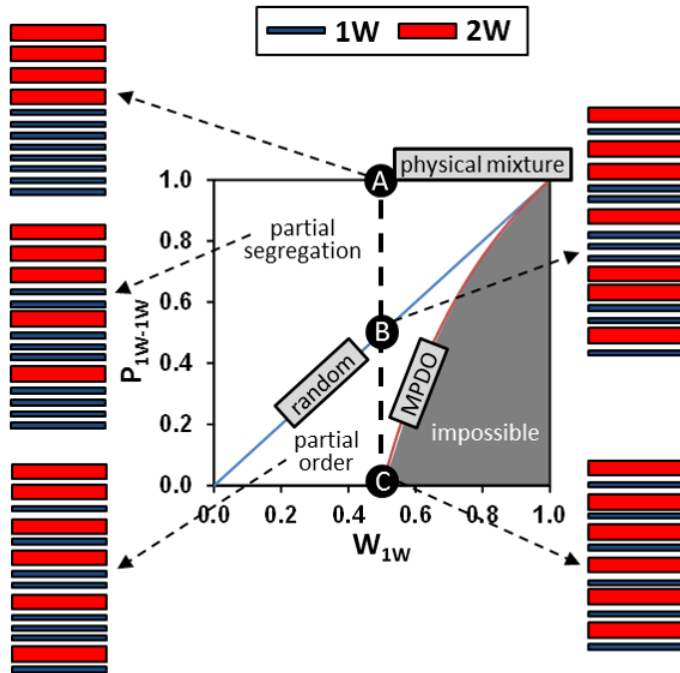


**Figure 3.** (Top) Junction probability diagram for  $R = 1$  mixed layers composed of 1W and 2W MXene layers (adapted from Bethke et al.<sup>32</sup>).  $W_{1W}$  and  $P_{1W-1W}$  stand for the relative proportion of 1W layers and the probability of finding two successive 1W layers, respectively. Mixed layers corresponding to physical mixture, random interstratification (i.e.,  $R = 0$ ), or maximum possible degree of ordering (MPDO) as well as partial segregation or partial ordering are shown with typical examples of layer stacking sequences. (Bottom) Calculated XRD patterns of mixed layers with equal proportions of 1W and 2W layers ( $W_{1W} = 0.5$ ) and different  $P_{1W-1W}$  parameters. **A:** physical mixture ( $P_{1W-1W} = 1$ ). **B:** random interstratification ( $P_{1W-1W} = W_{1W} = 0.5$ ). **C:** maximum possible degree of ordering (MPDO –  $P_{1W-1W} = 0$ ). The vertical gray bar indicates a modified intensity scale factor ( $\times 20$ ) for the high-angle region of the patterns. The vertical dashed gray lines and solid black lines indicate theoretical positions for  $00l$  reflections of periodic 2W and 1W MXenes, respectively.

Comparison between experimental and calculated XRD patterns taking into account hydration heterogeneity is shown in Figure 2, details on the fitting strategy being reported in Supporting Information.<sup>29</sup> Briefly, one periodic sequence of layer (1W or 2W) is used first to reproduce as much as possible of the data. If necessary, mixed layers containing 1W and 2W layers are added to the calculated profile. Up to four randomly interstratified mixed layers (each with different proportions 1W and 2W layers) were necessary to reproduce some of the experimental patterns owing to hydration heterogeneity leading to complex diffraction maxima with broad and asymmetric maxima. The use of several mixed layers to fit XRD data does not imply the actual presence of different populations of particles in the sample but rather indicates that hydration heterogeneities are not randomly distributed within MXene crystallites. Note that

an additional reflection at  $\sim 9$  Å with stable absolute intensity through the entire range of RH and assigned to marginal amounts of original MAX crystallites was not considered in the modeling exercise. Results of the fitting procedure are reported in Figure 4. Evolution of the relative abundance of 1W and 2W layers with RH (Figure 4A) evidences that hydration heterogeneity is almost systematic along the water vapor desorption isotherm. Indeed, interstratification seems to be the rule for MXene crystal-structure over the 10-95% RH range, with a smooth evolution and a noticeable amount of 1W layers present even at high RH values with 30% of 1W layers at RH = 95% (Figure 4A), consistent with the visible shoulder at  $\sim 12$  Å. This smooth evolution of layer proportions appears as contradictory to the abrupt transition between the two hydration states hypothesized from the evolution of 001 reflection position (Figure 2 and Ghidui et al.<sup>21</sup>). However, the position of the 001 reflection is only apparent and depends on many factors, including the size of coherent scattering domains<sup>30</sup> and interstratification (Figure 3). Both effects lead to a shift of the experimental position of the 001 reflection from the layer-to-layer distance expected for a periodic structure. Based on structure models obtained from the fit of XRD patterns, an actual mean value for layer-to-layer distance can be calculated as a weighted average of the layer-to-layer distances corresponding to 1W and 2W (Table S1). When compared to experimental positions of the most intense 001 reflection (Figure 4B in gray), the actual mean layer-to-layer distance (Figure 4B in black) significantly differs for most RH values. This finding shows again the smooth overall structure evolution of hydration process of MXene interlayers, far from the expected abrupt 1W-2W transition when considering only the most intense 001 reflection as reported Figure 4B in gray. The discrepancy between the actual mean layer-to-layer distance and the position of the most intense 001 reflection is maximum over RH corresponding to the transition between two “homogeneous” hydration states (40-60%RH). Over this RH range,

XRD patterns exhibit a clear doublet, indicative of specific order-disorder in the distribution of the different layer types.

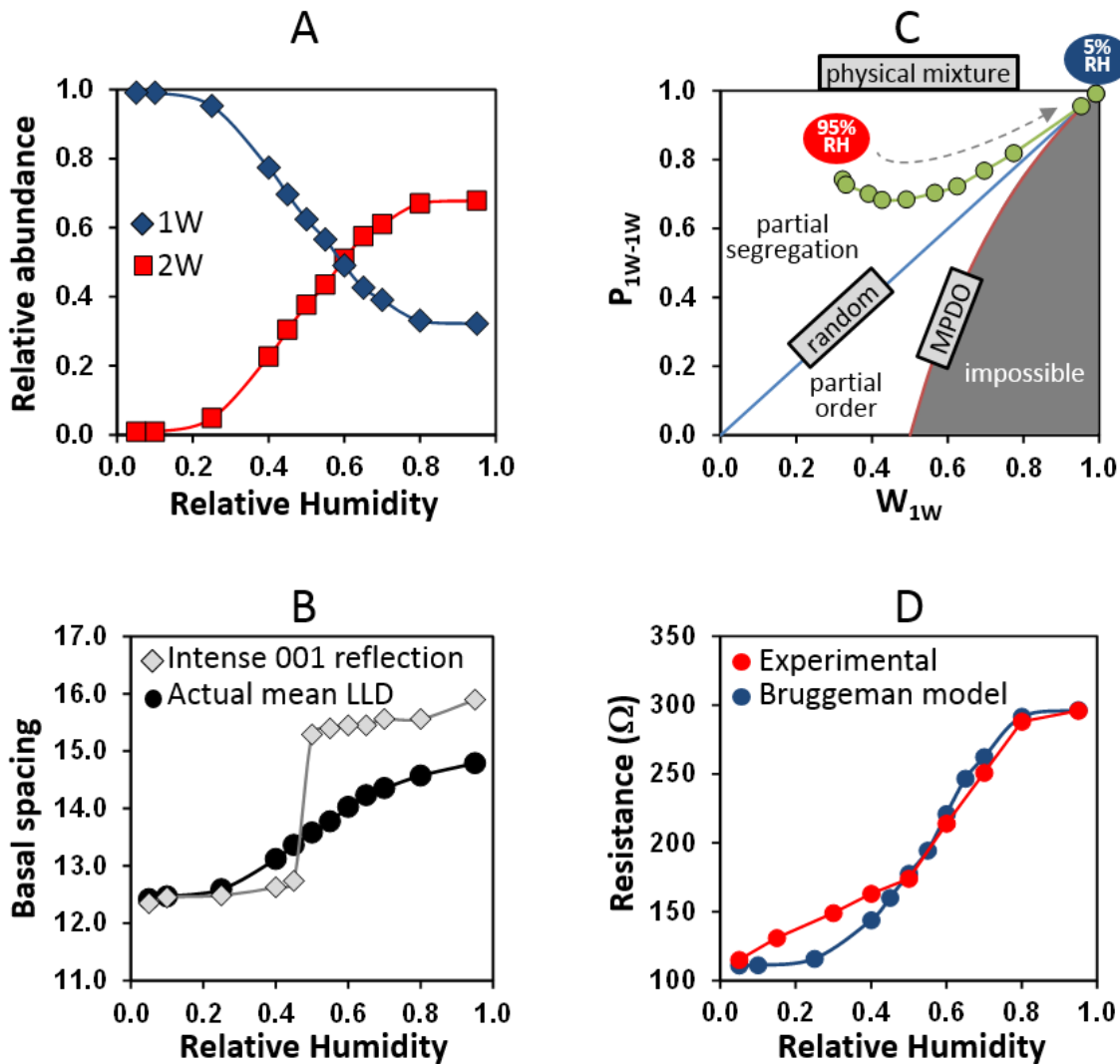


**Figure 4.** Evolution of MXene hydration along the water vapor desorption isotherm. **A:** Evolution of the relative proportions of 1W and 2W layers (summing up all mixed layers). **B:** Comparison between the weighted average actual mean layer-to-layer distance and the experimental position of the most intense 001 reflection. **C:** Projection of the structural disorder of MXene in the junction probability diagram for  $R = 1$  mixed layers (adapted from Bethke et al.<sup>32</sup>). **D:** Comparison between measured and computed resistances using Bruggeman model.

Additional information on the nature of the crystal-structure disorder can be obtained by recasting refined structure models on the junction probability diagram for  $R = 1$  mixed layers (Figure 4C).<sup>32</sup> For a combination of randomly interstratified mixed layers, the parameters  $W_{1W}$  and  $P_{1W-1W}$  can be computed as (Table S1):

$$W_{1W} = \sum_{i=1}^n [Ab.MLS^i \times (W_{1W}^i)] \quad (5)$$

and

$$P_{1W-1W} = \sum_{i=1}^n [Ab.MLS^i \times (W_{1W}^i)^2] / \sum_{i=1}^n [Ab.MLS^i \times (W_{1W}^i)] \quad (6)$$

where  $n$  stands for the number of mixed layers used to reproduce XRD data (from 2 to 4 depending on the RH value, see Table S1),  $Ab.MLS^i$  being the relative proportion of the  $i^{\text{th}}$  mixed layer and  $W_{1W}^i$  its 1W content. According to Figure 4C, all models systematically correspond to partial segregation, i.e., the succession of layers having the same hydration state is favored. Such segregated “domains” with contrasting hydration states are commonly observed for hydrated clays as smectite.<sup>34,35</sup>

**Influence of MXene hydration on its electrical properties.** In the previous section, we have evidenced the interstratification at stake in  $Ti_3C_2$  and determined relative proportions of 1W and 2W MXene layers as a function of RH by fitting XRD data. The impact of this hydration heterogeneity on the electrical resistivity of the material is now considered. Resistance measurements show a strong decrease of the resistance (from  $\sim 300$  to  $\sim 110 \Omega$ ) when RH is swept from 95% to 5% (Figure 4D). Such a strong dependence has already been reported<sup>36,37</sup> and is very promising for humidity sensor devices. It is also noticeable that the resistance does not evolve with RH for a  $Ti_3AlC_2$  MAX phase pellet (not shown) highlighting the crucial influence of the MXene clay-like material ability to insert water between the layers on electrical properties.



A simple model was used to assess the relation between hydration and resistance: the pellet is pictured as a homogeneous mixture of 1W- and 2W-MXene whose volumic proportions are derived from the analysis of XRD data. The effective resistance is then computed using an effective medium approximation in the framework of the Bruggeman model. The resistance of the 1W MXene is taken as the limit of the pellet resistance when RH tends to 0%, as in this case the proportion of 2W-MXene in the pellet tends to zero ( $R_{1W} = 110 \Omega$ ). Likewise, the resistance of the 2W-MXene is computed from the limit at RH = 100%, where %2W tends to 70% ( $R_{2W} = 530 \Omega$ ), leading to a resistance ratio of 4.8 between the two components. Although the Bruggeman model considers resistivity and not resistance, the above data processing is relevant as both parameters differ only by a fixed factor related to the geometry of the pellet and to its density, the latter being non-accessible. A fair agreement is obtained when comparing calculated and measured resistance data (Figure 4D). Hence, although simple, the two-component Bruggeman model captures the essence of the resistance variation relating it quantitatively to the proportion of 2W layers derived from XRD modeling. Taking account that the in-plane conductivity is greater than the out-of-plane conductivity and the low electronic conductivity of water, the increase of the layer-to-layer distance should increase the resistivity of the MXene material by disruption of conductivity, consistent with our results and those of Romer et al.<sup>36</sup>

## CONCLUSION

In this work, hydration heterogeneity is shown to prevail in  $Ti_3C_2T_x$  over a wide range of relative humidity. Whereas an abrupt transition of bihydrated to monohydrated MXene layers is commonly reported in the literature for these materials, we show that this transition can be rather a progressive one involving interstratification and partial segregation of layers having different

hydration states, as in clay minerals. As an example, the fraction of 1W MXene remains important even at high RH with 30% of 1W layers at 95% RH. Moreover, the specific XRD modelling approach used in the present study allows overcoming the intrinsic limitations of the Rietveld method related to the absence of periodicity and provides quantitative information on the relative proportions of the different layer types (1W and 2W) as a function of RH. This approach provides pivotal information for the characterization of these materials, and for the prediction of their properties, the presence of interlayer cations and/or water molecules being key to applications such as humidity sensors, electrochemistry (battery, supercapacitor,...), optical devices, water purification, etc. In the present study, the key role of hydration heterogeneity is exemplified on  $\text{Ti}_3\text{C}_2\text{T}_x$  by the direct relation existing between the fraction of 1W layers and resistivity whereas consideration of an abrupt 1W-2W transition would have led to poor reproduction of experimental data.

Taking account that MXene hydration (and therefore, the interstratification behavior) depends undoubtedly on the nature of the inserted cation as well as on the nature of terminal groups, the proposed approach appears as very complementary to usual methods such as XPS or NMR to characterize these materials which possess a very complex chemistry. The proposed approach should be especially useful to decipher the nature and the amount of terminal groups, their compositional evolution with the synthesis and/or post-treatment processes. Indeed, the determination of these species is still a drag in the understanding of MXene surface chemistry.

Finally, this work provides important foundations to the MXene community for the interpretation of the complex XRD patterns obtained on these materials which sometimes vary widely from a synthesis to another due to various experimental parameters (etching environment, storage and drying conditions, post-treatment, etc).

## EXPERIMENTS AND METHODS

**Synthesis of  $Ti_3C_2T_x$ .** The synthesis of Li-saturated  $Ti_3C_2T_x$  powder is based on the work of Ghidui et al.<sup>21</sup> 1g of LiCl ( $\geq 99\%$ , Sigma) was added to 10 mL of an aqueous HF solution (12%wt, prepared from aqueous HF  $\geq 48\%$ , Sigma-Aldrich). After dissolution of LiCl, 1g of  $Ti_3AlC_2$  powder (see Wang et al.<sup>6</sup> for the synthesis of MAX phase – initial particles sizes  $<25 \mu m$ ) was progressively introduced into the solution to avoid initial overheating. The mixture was then stirred at  $25^\circ C$  for 24h. After this step, the suspension was centrifuged to remove the supernatant and washed 3 times with 80 mL of HCl 6M by centrifugation. The powder was then added to 80 mL of a deaerated solution of LiCl 1M for 1h and a second time for 24h after centrifugation. During these processes, the deaerated solutions were maintained under argon to avoid potential oxidation with dissolved oxygen as already observed on MXenes.<sup>6</sup> Finally, the solution was washed with 80 mL of ultrapure water by centrifugation (3 times), filtered and dried for 24h under air to collect Li-saturated  $Ti_3C_2T_x$  powder.

**XRD analysis of  $Ti_3C_2T_x$  powder.** XRD analysis of the MXene powder was carried out with a PANalytical EMPYREAN powder diffractometer using  $CuK\alpha$  radiation source ( $K\alpha_1 = 1.5406 \text{ \AA}$  and  $K\alpha_2 = 1.5444 \text{ \AA}$ ). XRD patterns were collected between  $5$  and  $70^\circ$  with a  $0.07^\circ$  step and 420 s dwell time at each step.

**XRD under controlled relative humidity and profile modeling of  $00l$  reflections.** For XRD analysis along the desorption isotherm, a fraction of the Li-saturated  $Ti_3C_2T_x$  powder was first dispersed in deaerated water as then dried on a glass slide. This preparation allowed optimizing preferred orientation of the platelets to enhance the intensity of  $00l$  reflections. XRD data collection was performed on a Bruker D8 diffractometer equipped with a MHG Messtechnik humidity controller coupled to an Anton Paar CHC+ chamber. A humidified  $N_2$  gas

was used to minimize sample oxidation during data collection. Intensities were collected for 4 s per  $0.04^{\circ}2\theta$  step over the  $3\text{--}32^{\circ}2\theta$   $\text{CuK}\alpha$  angular range with a SolXE Si (Li) solid state detector. Experimental setup included divergence slits, the two Soller slits, the antiscatter, and resolution slits at  $0.3$ ,  $2.3$ ,  $0.3$  and  $0.1^{\circ}$ , respectively. MXene sample was first equilibrated at 98% relative humidity (RH) for more than 12h before decreasing in a stepwise manner the RH down to 5%. For each humidity step the sample was left to equilibrate during 1h before XRD data collection. Hydration stability during data collection was checked by collecting XRD data again for the 001 reflection.

Modeling of experimental 00 $l$  reflections was performed using the algorithms developed by Sakharov et al.<sup>38</sup> for mixed layers. Instrumental and experimental factors (horizontal and vertical beam divergences, goniometer radius, sample length and thickness, mass absorption coefficient) were introduced without further adjustment. Additional parameters included the layer-to-layer distance of monohydrated (1W) or bihydrated (2W) MXene layers taken as the distance between two successive layers (Figure 1) and the coherent scattering domain size along the  $c^*$  axis, characterized by a maximum value, set to 50 layers, and by a variable mean value ( $N$ ).  $z$ -coordinates proposed by Shi et al.<sup>39</sup> for the  $\text{Ti}_3\text{C}_2$  layer were used without further adjustment. For 1W layers, interlayer water molecules were introduced as a single plane located at the interlayer mid-plane. For 2W state, water molecules were distributed as two planes located at a distance of  $\pm 1.2 \text{ \AA}$  from the interlayer mid-plane, similar to the equilibrium positions reported in hydrated clay minerals.<sup>40</sup> Given the low electronic content of Li atoms and the related insensitivity of XRD towards these elements, they were not included in the interlayer model.

**Resistance measurements.** Resistance measurements were performed under nitrogen and controlled humidity (VTI RH-100 humidity generator device) from 98 %RH to 5%RH on a

Ti<sub>3</sub>C<sub>2</sub>T<sub>x</sub> pellet prepared from Ti<sub>3</sub>C<sub>2</sub>T<sub>x</sub> powders. The resistance of the pellet was monitored with a Keithley 2700 multimeter in a 4-probe Van der Pauw configuration, with copper wires attached to the pellet using silver paint. For each resistance measurement, the sample was left to equilibrate for 3h. This duration was sufficient to stabilize the resistance of the pellet and consequently, to obtain a stable structural rearrangement for a given RH value.

## ASSOCIATED CONTENT

### **Supporting Information (separate file)**

Description of MXene synthesis with the XRD pattern of as-prepared Ti<sub>3</sub>C<sub>2</sub>T<sub>x</sub> MXene (Figure S1); Description of the fitting strategy for the modeling of experimental XRD patterns and comparison between the experimental and calculated XRD patterns of 00 $l$  reflections for Li-saturated Ti<sub>3</sub>C<sub>2</sub>T<sub>x</sub> MXene as a function of relative humidity (RH) (Figure S2). Structural parameters used to reproduce experimental X-ray diffraction patterns of Li-saturated Ti<sub>3</sub>C<sub>2</sub>T<sub>x</sub> MXene as a function of relative humidity (Table S1).

## AUTHOR INFORMATION

### **Corresponding Authors**

\* E-mail: [stephane.celerier@univ-poitiers.fr](mailto:stephane.celerier@univ-poitiers.fr), [eric.ferrage@univ-poitiers.fr](mailto:eric.ferrage@univ-poitiers.fr)

## ACKNOWLEDGMENTS

IC2MP through ATI project (“Action Transversale Incitative” 2017), the European Union (ERDF), the “Région Nouvelle Aquitaine” and the French research ministry (Ph.D. thesis of M. Benchakar) are gratefully acknowledged for financial support. This work also partially pertains to the French Government program “Investissements d’Avenir” (LABEX INTERACTIFS, reference ANR-11-LABX-0017-01) which is here gratefully acknowledged for the financial support to C. Garnero post-doctoral position. ISTERre is part of Labex OSUG@2020 (ANR10 LABX56).

## REFERENCES

- (1) Bhimanapati, G. R.; Lin, Z.; Meunier, V.; Jung, Y.; Cha, J.; Das, S.; Xiao, D.; Son, Y.; Strano, M. S.; Cooper, V. R.; Liang, L.; Louie, S. G.; Ringe, E.; Zhou, W.; Kim, S. S.; Naik, R. R.; Sumpter, B. G.; Terrones, H.; Xia, F.; Wang, Y.; Zhu, J.; Akinwande, D.; Alem, N.; Schuller, J. A.; Schaak, R. E.; Terrones, M.; Robinson, J. A. Recent Advances in Two-Dimensional Materials beyond Graphene. *ACS Nano* **2015**, *9*, 11509-11539.
- (2) Novoselov, K. S.; Geim, A. K.; Morozov, S. V.; Jiang, D.; Zhang, Y.; Dubonos, S. V.; Grigorieva, I. V.; Firsov, A. A. Electrical Field Effect in Atomically Thin Carbon Films. *Science* **2004**, *306*, 666-669.
- (3) Naguib, M.; Mochalin, V. N.; Barsoum, M. W.; Gogotsi, Y. 25<sup>th</sup> anniversary article: MXenes: a new family of two-dimensional materials. *Adv. Mater.* **2014**, *26*, 992-1005.
- (4) Ghidoui, M.; Lukatskaya, M. R.; Zhao, M.-Q.; Gogotsi, Y.; Barsoum, M. W. Conductive two-dimensional titanium carbide 'clay' with high volumetric capacitance. *Nature* **2014**, *516*, 78.
- (5) Barsoum, M. W. In *MAX Phases: Properties of Machinable Ternary Carbides and Nitrides*; Wiley-VCH Verlag GmbH: 2013, pp 237-269.
- (6) Wang, X.; Garnero, C.; Rochard, G.; Magne, D.; Morisset, S.; Hurand, S.; Chartier, P.; Rousseau, J.; Cabioc'h, T.; Coutanceau, C.; Mauchamp, V.; Célérier, S. A new environment (FeF<sub>3</sub>/HCl) for the synthesis of two-dimensional titanium carbide MXenes: a route towards selective reactivity vs. water. *J. Mater. Chem. A* **2017**, *5*, 22012-22023.

- (7) Naguib, M.; Kurtoglu, M.; Presser, V.; Lu, J.; Niu, J.; Heon, M.; Hultman, L.; Gogotsi, Y.; Barsoum, M. W. Two-Dimensional Nanocrystals Produced by Exfoliation of  $\text{Ti}_3\text{AlC}_2$ . *Adv. Mater.* **2011**, *23*, 4248-4253.
- (8) Shahzad, F.; Alhabeab, M.; Hatter, C. B.; Anasori, B.; Man Hong, S.; Koo, C. M.; Gogotsi, Y. Electromagnetic interference shielding with 2D transition metal carbides (MXenes). *Science* **2016**, *353*, 1137-1140.
- (9) Anasori, B.; Lukatskaya, M. R.; Gogotsi, Y. 2D metal carbides and nitrides (MXenes) for energy storage. *Nat. Rev. Mater.* **2017**, *2*, 16098.
- (10) Zhang, X.; Lei, J.; Wu, D.; Zhao, X.; Jing, Y.; Zhou, Z. A Ti-anchored  $\text{Ti}_2\text{CO}_2$  monolayer (MXene) as a single-atom catalyst for CO oxidation. *J. Mater. Chem. A* **2016**, *4*, 4871-4876.
- (11) Guo, Z.; Zhou, J.; Zhu, L.; Sun, Z. MXene: a promising photocatalyst for water splitting. *J. Mater. Chem. A* **2016**, *4*, 11446-11452.
- (12) Hu, Q.; Sun, D.; Wu, Q.; Wang, H.; Wang, L.; Liu, B.; Zhou, A.; He, J. MXene: A New Family of Promising Hydrogen Storage Medium. *J. Phys. Chem. A* **2013**, *117*, 14253-14260.
- (13) Wang, F.; Yang, C.; Duan, M.; Tang, Y.; Zhu, J.  $\text{TiO}_2$  nanoparticle modified organ-like  $\text{Ti}_3\text{C}_2$  MXene nanocomposite encapsulating hemoglobin for a mediator-free biosensor with excellent performances. *Biosens. Bioelectron.* **2015**, *74*, 1022-1028.
- (14) Ying, G.; Dillon, A. D.; Fafarman, A. T.; Barsoum, M. W. Transparent, conductive solution processed spincoated 2D  $\text{Ti}_2\text{CT}_x$  (MXene) films. *Mater. Res. Lett.* **2017**, *5*, 391-398.
- (15) Come, J.; Black, J. M.; Lukatskaya, M. R.; Naguib, M.; Beidaghi, M.; Rondinone, A. J.; Kalinin, S. V.; Wesolowski, D. J.; Gogotsi, Y.; Balke, N. Controlling the actuation properties of MXene paper electrodes upon cation intercalation. *Nano Energy* **2015**, *17*, 27-35.
- (16) Ren, C. E.; Hatzell, K. B.; Alhabeab, M.; Ling, Z.; Mahmoud, K. A.; Gogotsi, Y. Charge- and Size-Selective Ion Sieving Through  $\text{Ti}_3\text{C}_2\text{T}_x$  MXene Membranes. *J. Phys. Chem. Lett.* **2015**, *6*, 4026-4031.
- (17) Osti, N. C.; Naguib, M.; Ostadhossein, A.; Xie, Y.; Kent, P. R. C.; Dyatkin, B.; Rother, G.; Heller, W. T.; van Duin, A. C. T.; Gogotsi, Y.; Mamontov, E. Effect of Metal Ion

Intercalation on the Structure of MXene and Water Dynamics on its Internal Surfaces. *ACS Appl. Mater. Interfaces* **2016**, *8*, 8859-8863.

(18) Lei, J.-C.; Zhang, X.; Zhou, Z. Recent advances in MXene: Preparation, properties, and applications. *Front. Phys.* **2015**, *10*, 276-286.

(19) Hong Ng, V. M.; Huang, H.; Zhou, K.; Lee, P. S.; Que, W.; Xu, J. Z.; Kong, L. B. Recent progress in layered transition metal carbides and/or nitrides (MXenes) and their composites: synthesis and applications. *J. Mater. Chem. A* **2017**, *5*, 3039-3068.

(20) Wang, H.; Wu, Y.; Yuan, X.; Zeng, G.; Zhou, J.; Wang, X.; Chew, J. W. Clay-Inspired MXene-Based Electrochemical Devices and Photo-Electrocatalyst: State-of-the-Art Progresses and Challenges. *Adv. Mater.* **2018**, *30*, 1704561.

(21) Ghidui, M.; Halim, J.; Kota, S.; Bish, D.; Gogotsi, Y.; Barsoum, M. W. Ion-Exchange and Cation Solvation Reactions in  $Ti_3C_2$  MXene. *Chem. Mater.* **2016**, *28*, 3507-3514.

(22) Moore, D. M.; Reynolds, R. C., Jr *X-ray Diffraction and the Identification and Analysis of Clay Minerals*; Oxford University Press: Oxford, 1997.

(23) Bradley, W. F.; Grim, R. E.; Clark, G. F. A Study of the Behavior of Montmorillonite upon Wetting. *Z. Kristallogr.* **1937**, *97*, 216-222.

(24) Nagelschmidt, G. On the Lattice Shrinkage and Structure of Montmorillonite. *Z. Kristallogr.* **1936**, *93*, 481-487.

(25) Shpigel, N.; Levi, M. D.; Sigalov, S.; Mathis, T. S.; Gogotsi, Y.; Aurbach, D. Direct Assessment of Nanoconfined Water in 2D  $Ti_3C_2$  Electrode Interspaces by a Surface Acoustic Technique. *J. Am. Chem. Soc.* **2018**, *140*, 8910-8917.

(26) Ghidui, M.; Kota, S.; Halim, J.; Sherwood, A. W.; Nedfors, N.; Rosen, J.; Mochalin, V. N.; Barsoum, M. W. Alkylammonium Cation Intercalation into  $Ti_3C_2$  (MXene): Effects on Properties and Ion-Exchange Capacity Estimation. *Chem. Mater.* **2017**, *29*, 1099-1106.

(27) Hu, M.; Hu, T.; Li, Z.; Yang, Y.; Cheng, R.; Yang, J.; Cui, C.; Wang, X. Surface Functional Groups and Interlayer Water Determine the Electrochemical Capacitance of  $Ti_3C_2T_x$  MXene. *ACS Nano* **2018**, *12*, 3578-3586.

(28) Dillon, A. D.; Ghidui, M. J.; Krick, A. L.; Griggs, J.; May, S. J.; Gogotsi, Y.; Barsoum, M. W.; Fafarman, A. T. Highly Conductive Optical Quality Solution-Processed Films of 2D Titanium Carbide. *Adv. Funct. Mater.* **2016**, *26*, 4162-4168.



- (29) Ferrage, E.; Lanson, B.; Michot, L. J.; Robert, J. L. Hydration Properties and Interlayer Organization of Water and Ions in Synthetic Na-Smectite with Tetrahedral Layer Charge. Part 1. Results from X-ray Diffraction Profile Modeling. *J. Phys. Chem. C* **2010**, *114*, 4515-4526.
- (30) Drits, V. A.; Tchoubar, C. *X-ray diffraction by disordered lamellar structures: Theory and applications to microdivided silicates and carbons*; Springer-Verlag: Berlin, 1990.
- (31) Jagodzinski, H. Eindimensionale Fehlordnung in Kristallen und ihr Einfluss auf die Röntgeninterferenzen. I. Berechnung des Fehlordnungsgrades aus den Röntgenintensitäten. *Acta Crystallogr.* **1949**, *2*, 201-207.
- (32) Bethke, C. G.; Vergo, N.; Altaner, S. P. Pathways of smectite illitization. *Clays & Clay Miner.* **1986**, *34*, 125-135.
- (33) Méring, J. L'interférence des rayons X dans les systèmes à stratification désordonnée. *Acta Crystallogr.* **1949**, *2*, 371-377.
- (34) Dazas, B.; Lanson, B.; Breu, J.; Robert, J. L.; Pelletier, M.; Ferrage, E. Smectite fluorination and its impact on interlayer water content and structure: A way to fine tune the hydrophilicity of clay surfaces? *Micropor. Mesopor. Mater.* **2013**, *181*, 233-247.
- (35) Ferrage, E.; Tournassat, C.; Rinnert, E.; Lanson, B. Influence of pH on the interlayer cationic composition and hydration state of Ca-montmorillonite: Analytical chemistry, chemical modelling and XRD profile modelling study. *Geochim. Cosmochim. Acta* **2005**, *69*, 2797-2812.
- (36) Römer, F. M.; Wiedwald, U.; Strusch, T.; Halim, J.; Mayerberger, E.; Barsoum, M. W.; Farle, M. Controlling the conductivity of Ti<sub>3</sub>C<sub>2</sub> MXenes by inductively coupled oxygen and hydrogen plasma treatment and humidity. *RSC Adv.* **2017**, *7*, 13097-13103.
- (37) Muckley, E. S.; Naguib, M.; Wang, H.-W.; Vlcek, L.; Osti, N. C.; Sacci, R. L.; Sang, X.; Unocic, R. R.; Xie, Y.; Tyagi, M.; Mamontov, E.; Page, K. L.; Kent, P. R. C.; Nanda, J.; Ivanov, I. N. Multimodality of Structural, Electrical, and Gravimetric Responses of Intercalated MXenes to Water. *ACS Nano* **2017**, *11*, 11118-11126.
- (38) Sakharov, B. A.; Naumov, A. S.; Drits, V. A. X-ray diffraction by mixed-layer structures with random distribution of stacking faults. *Dokl. Akad. Nauk.* **1982**, *265*, 339-343 (in Russian).

(39) Shi, C.; Beidaghi, M.; Naguib, M.; Mashtalir, O.; Gogotsi, Y.; Billinge, S. J. L. Structure of Nanocrystalline  $Ti_3C_2$  MXene Using Atomic Pair Distribution Function. *Phys. Rev. Lett.* **2014**, *112*, 125501.

(40) Ferrage, E. Investigation of the interlayer organization of water and ions in smectite from the combined use of diffraction experiments and molecular simulations. A review of methodology, applications, and perspectives. *Clays & Clay Miner.* **2016**, *64*, 348-373.

## TABLE OF CONTENT

